12WCEE 2000

ESTIMATION OF HIGH-FREQUENCY WAVE RADIATION AREAS ON THE FAULT PLANE OF THE 1994 SANRIKU-HARUKA-OKI EARTHQUAKE

S KURITA[1] And Mitugu TAKITA[2]

SUMMARY

We investigated the high-frequency wave radiation process of the 1994 Sanriku-Haruka-Oki earthquake (Mw = 7.7) and the accumulated tectonic stress on the source region. The rupture process was estimated from an envelope inversion of acceleration seismograms. The large high-frequency waves were radiated at the edges of the fault plane and at the near edges of the large slipped areas. This result suggests that stopping of rupture causes the high-frequency wave radiation. The accumulated tectonic stress on the fault plane in a time interval was calculated with a 2-D finite element model. The distribution pattern of accumulated stress on the western part of the fault plane is similar to that of slip. One of the possible explanations of the result is that the asperities on the western fault plane are characteristic asperities. From the comparison with the distributions of accumulated stress and high-frequency wave radiation intensity, it is indicated that the spatial variation in accumulated stress in the area of asperity affects the intensity of high-frequency wave radiation.

INTRODUCTION

Prediction methods for strong ground motion such as an empirical Green's function method sometimes can not reproduce observed acceleration seismograms in which high-frequency (higher than 1Hz) waves are predominant, even if inhomogeneous slips of a fault are taken into account. Improvements of the prediction methods in accuracy are necessary to clarify the radiation processes of high-frequency wave on a fault plane. Kakehi et al. (1996a, 1996b, 1997) analysed the recent large earthquakes occurred in Japan with an envelope inversion method of acceleration seismograms. They found that the areas of high- and low-frequency wave radiation on the fault plane were not correlated. It is considered that their finding is important to improve the prediction methods.

We investigate the high-frequency wave radiation process of the 1994 Sanriku-Haruka-Oki earthquake (Mw = 7.7) and the accumulated tectonic stress on the source region by analysing the observed seismograms and performing numerical simulation. The earthquake occurred at 21:19 in local time on 28 December 1994, which occurred far off the northeast coast of Tohoku region, the northern part of Japan. Large-amplitude high-frequency waves were recorded at many stations. First, the rupture process is estimated by applying the envelope inversion method [Kakehi and Irikura (1996a)] to the acceleration seismograms of the main shock. The high-frequency wave radiation process is examined by comparing the inversion results with the slip distribution on the fault plane obtained by Nakayana and Takeo (1997). Next, the accumulated tectonic stress on the source region is calculated with the 2-D finite element model. We examine the relationship among the accumulated stress, the slip, and the high-frequency wave radiation in conjunction with asperity and barrier.

[1] *Dept of Architecture and Building Science, School of Engineering Tohoku Uni Email:kurita@strmech.archi.tohoku.ac.jp*
[2] *Department of Architecture Hachinohe Institute of Technology, Japan Email: takita@hi-tech.ac.jp*

INVERSION

Method

The acceleration radiation intensities and the rupture times of the 1994 Sanriku-Haruka-Oki earthquake are estimated with the envelope inversion method developed by Kakehi and Irikura (1996a). The inversion method is based on the minimum least-squares estimation method. The mean-square estimation error function is defined with the difference between envelopes of observed seismogram and synthetic acceleration waveform. The synthetic acceleration waveform $\overline{A}(t)$ is a function of the estimated parameters. $\overline{A}(t)$ is calculated by using the empirical Green' function method expressed as follows:

$$\overline{A}(t) = c\sum_{i=1}^{N_X}\sum_{j=1}^{N_Y} w_{ij}\frac{r}{r_{ij}}F_{ij} * a(t) \quad \cdots (1) \qquad F_{ij} = \delta(t-t_{ij}) + \frac{1}{n'}\sum_{k=1}^{(N_T-1)m'}\delta\left(t - t_{ij} - \frac{(k-1)\tau_L}{(N_T-1)n'}\right) \cdots (2)$$

$$t_{ij} = (r_{ij} - r_0)/\beta + s_{ij} \quad \cdots (3)$$

Here, N_X and N_Y are the division numbers of a fault plane along the strike direction and along the dip direction respectively. c is the stress-drop ratio between large and small events. τ_L is the rise time of the large event. N_T is the division number of τ_L. r_{ij} is the distance from subfault (i, j) to a station. β is the S-wave velocity. $a(t)$ is the acceleration seismogram of the small event used as an empirical Green' function. r, r_0, and r_{ij} are the hypocentral distances of the small event, the large event, and subfault (I, j) respectively. n' is a parameter for removing the artificial period. w_{ij} and s_{ij} are the acceleration radiation intensity and the rupture time of subfault (i, j) respectivley. The acceleration radiation intensity is regarded as the strength of high-frequency wave radiation.

Our calculation procedure for the envelope of waveform is different from theirs. We apply the moving average window to the amplitude of the complex envelopes of observed and synthetic waveforms. The complex envelopes are calculated with FFT. The time window length of 1 sec is used for moving average operation.

DATA AND FAULT MODEL

The acceleration seismograms of the main shock were recorded at a large number of stations in the northern part of Japan. However, the seismograms of the aftershocks suitable for the envelope inversion were recorded at a small number of stations. Because of this limitation, we use the acceleration seismograms recorded at only a station which is in the campus of HIT (Hachinohe institute of technology). The location of the station is illustrated in Figure 1. The seismograms of more than ten aftershocks were recorded at this station. The acceleration seismograms of the aftershock of which the source mechanism is every similar to that of the main shock are used as the empirical Green' function. The magnitude of the aftershock is M_{JMA} 5.4. The CMT solutions of the main shock and the aftershock are shown in Table 1.

The geometry and the location of the fault plane are determined from the fault model which Nakayama and Takeo (1997) constructed for the waveform inversion of the 1994 Sanriku-Haruka-Oki earthquake. Their fault model consists of three fault planes with the same strike of $N180^\circ S$ and the different dip angles. The dip angle in the shallow region is 6°. The angles in middle of the fault plane and in the deep region are 18° and 30° respectively. We simplify their fault model to the two fault planes with the different dip angles. The fault model is shown in Figure 1. The area of the fault plane $(110km \times 170km)$ is the same as theirs. We determine $N_X = 8, \quad N_Y = 6, \quad N_T = 7, \quad c = 7.14$ from the ratios in seismic moment and spectrum in a high-frequency range between the aftershock to the main shock.

To examine the influence of the initial values on inversion results, we consider the two cases of initial values of rupture time shown in Figure 2. The initial values are calculated from the following rupture velocities in the condition that the rupture propagates concentrically from the epicenter determined by JMA (Japan Meteorological Agency).

1) case-1: $V_{r1} = 2.79km/s, \quad V_{r2} = 2.79km/s$

2) case-2: $V_{r1} = 2.58km/s, \quad V_{r2} = 3km/s$

Here, V_{r1} and V_{r2} are the rupture velocities on the eastern fault plane and on the western fault plane respectively. The rupture velocities of case-1 are determined from the results of Kato et al. (1996). They analysed the acceleration seismograms of the main shock recorded at a number of JMA stations. They obtained the following relationships for the rupture propagation:

$L / v_r = 53\text{sec}, \quad v_r / \beta = 0.62, \quad \phi = W9^\circ N$ ...(4)

Table 1: CMT Solutions and JMA magnitude

	Date	Time	Lat	Long	Depth	Moment	Strike	Dip	Rake	Mjma
			Degree	Degree	km	dyne• cm	Degree	Degree	Degree	
Mainshock	94.12.28	21:19	40.56	142.99	14.8	4.90E+27	179	12	67	7.5
Aftershock	94.12.30	0:29	40.66	142.42	60.7	2.00E+24	181	25	64	5.4

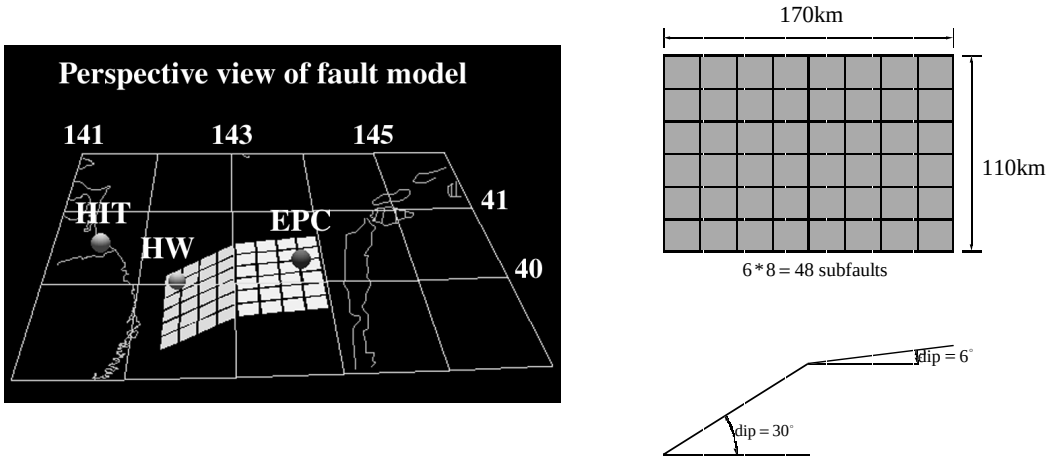

Figure 1: Fault model employed in the envelope inversion (EPC: the epicenter by JMA, HW: high-frequency source, HIT: Hachinohe insitute of technology)

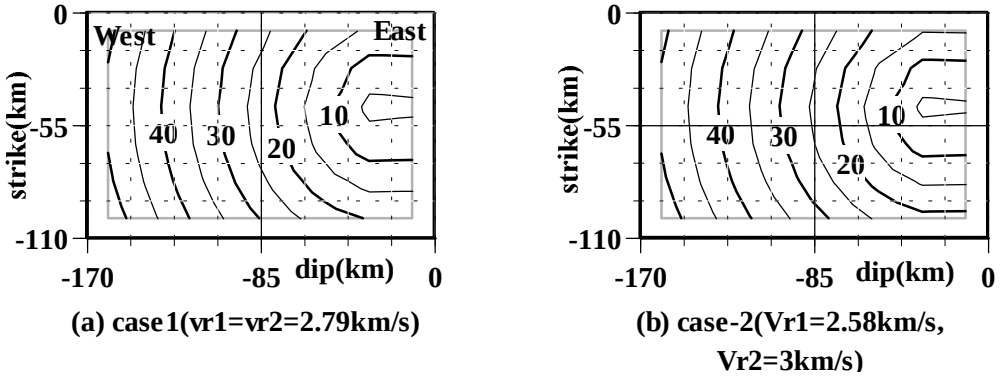

Figure 2: Distribution of initial values of rupture times for the inversion on the fault plane

Here, L is the fault length measured from the epicenter determined by JMA, v_r is the rupture velocity, ϕ is the direction of rupture propagation. The values of v_r and β are calculated by putting the length of our model to

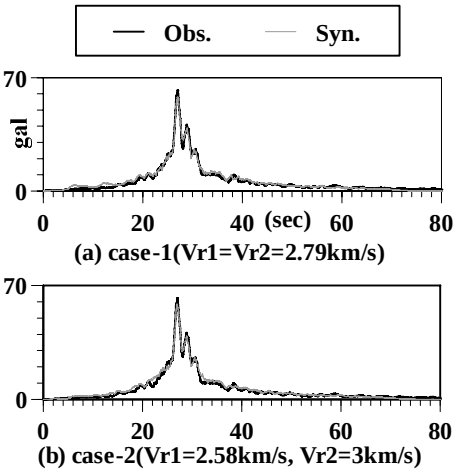

Figure 3: Comparison of the observed envelopes (Obs.) and the synthetic ones (Syn.) for the final solutions

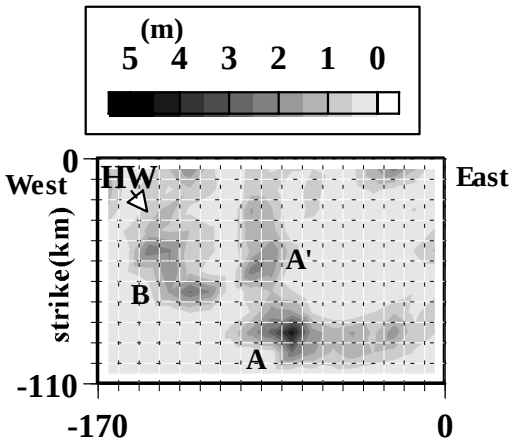

Figure 6: Slip distribution obtained from the waveform inversion (Nakayama and Takeo (1997)

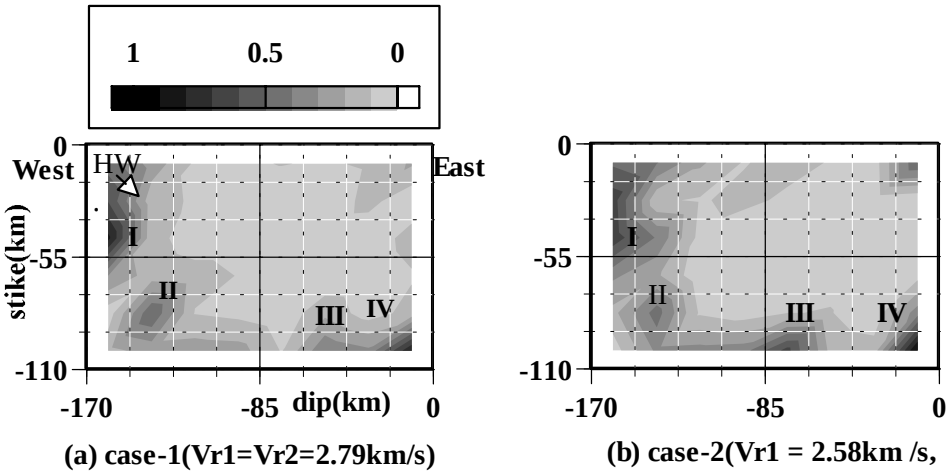

Figure 4: Distribution of acceleration radiation intensity on the fault plane

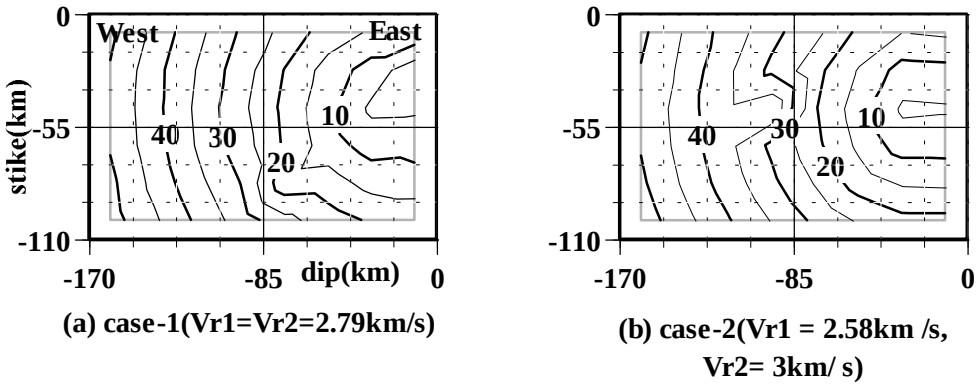

Figure 5: Distribution of rupture time on the fault plane

Eq. (4).

$$v_r = 2.79 km/s, \quad \beta = 4.5 km/s \quad \ldots(5)$$

The values of case-2 are determined from the results of Nakamura et al. (1997). According to their results, the rupture velocities on the eastern part and the western part of the fault are 1.8 km/s and 3.0km/s respectively. The value of V_{r1} was determined so that the rupture duration time equals to that of the case-1 (53 sec). The rise times of 3 sec and the shear wave velocity of 4.5km/s are used in the inversion. We perform the envelope inversion with the NS components of the seismograms.

Results

Figure 3 shows the comparison of the observed envelope and the synthetic one for the final solutions. The solutions for both cases reproduced the observed envelope very well. The acceleration radiation intensities and the rupture times are shown in Figure 4 and 5 respectively. Large high-frequency wave radiated in the four areas which are marked with labels I, II, III, and IV in Figure 4. HW denoted in Figure 4 is the location of the source of high-frequency wave determined from the S-wave arrival times by Nakayama et al. (1997). The high-frequency wave source is near to the area I at the western edge of the fault plane. The spatial resolution of our fault model is 21.25km in the dip direction and 18.33km in the strike direction. Taking into account a lack of spatial resolution in the inversion result, area I is considered to coincide with HW. Sato et al. (1997) analysed the different acceleration records of the 1994 Sanriku-Haruka-Oki earthquake with the different inversion method and the different fault model. Their result showed that high-frequency waves radiated mainly at the western edge of the fault plane. This coincides with our results. The presence of area II, III and IV is a difference between their results and ours.

Figure 6 shows the slip distribution obtained from the waveform inversion by Nakayama and Takeo (1997). Large slips are concentrated in the three asperities, A, A', and B illustrated in the same figure. The maximum slips of 4.4m occurred in the area of asperity A. Areas II and III lie at the near edge of asperities A and B respectively. The high-frequency waves radiate very small in the areas of those asperities. This result is similar to that of Kakehi et al. (1996a, 1996b, 1997). They analysed the strong motions of the 1993 Kushiro-Oki earthquake, the 1993 Hokkaido-Nansei-Oki earthquake, and the 1995 Hyogo-Ken Nanbu Earthquake occurred in Japan. Their result showed that the high-frequency wave radiation was large at the edges of fault plane and asperities. They interpreted this to be associated with stopping of rupture. It is also considered that the stopping of rupture generates the large high-frequency wave radiation of the 1994 Sanriku-Haruka-Oki earthquake. Nakayama and Takeo gave the possible two causes of the strong high-frequency radiation during the stopping of rupture: one is a high stress concentration due to the rapid slip changing, another is a stopping phase radiated from an abrupt change of rupture velocity. The rupture times in areas I, II, III and IV are similar to the initial values of the rupture times shown in Figure 2. This result is due to the lack of spatial resolution of our model as mentioned above. We cannot specify the cause of the high-frequency wave radiation from our inversion results.

STRESS ACCUMLATION

Modelling

We calculate the shear stress accumulation for tectonic loading from the visco-elastic analysis with the finite element method (FEM). Sato (1987) analysed the tectonic stress field in the northern part of Japan with the 3-D FEM. We simplify his model to the 2-D finite element model. The modelling is the same as Sato. The outline of the modelling is illustrated in Figure 7. The Japan Sea Plate and the Pacific Plate move in the direction of $N85^{\circ}E$ with a velocity $\dot{u}_{JP}$ of 1cm/yr and in the direction of $N70^{\circ}W$ with a velocity $\dot{u}_{PP}$ of 10cm/yr respectively. The movement of the Pacific Plate and Japan Sea Plate compresses the northeastern Japan Island Arc. We construct the computational model of the northeastern Japan Island Arc with the finite elements. The prescribed displacements corresponding to the plate velocities are imposed upon the nodes on the plate boundaries. The values of the displacements are calculated from the plate velocities in the parallel direction to the analytical plane of the model. In this calculation, a strength of seismic-coupling (seismic-coupling factor) between the Japan Island Arc and the Pacific Plate is taken into account. We consider the two cases of the seismic-coupling factor C_f : one is a uniform coupling, another is the seismic-coupling factor as a function of distance from the Japan Trench. Sato (1987) determined the latter:

$$\dot{u}_p = C_f \dot{u}_{pp} \quad where \quad C_f = \begin{cases} 0.3 & for \quad case-a \\ 0.42\exp(-3.1l/L)+0.78 & for \quad case-b \end{cases} \quad \ldots(6)$$

Here, l and L are the distances from the trench axis to the position and to the aseisimic front (A.F) respectively. C_f of case-b decrease as the distance from the trench axis becomes longer. The case-b was determined on the fact that large earthquakes occurred in the northern part of Japan in the latitude of more than $38^\circ N$ are relative near to the trench axis. The bottom of the model is fixed in the vertical direction. Figure 8 shows the mesh of the model. The numbers of the nodes and of the elements is 650 and 560 respectively. The

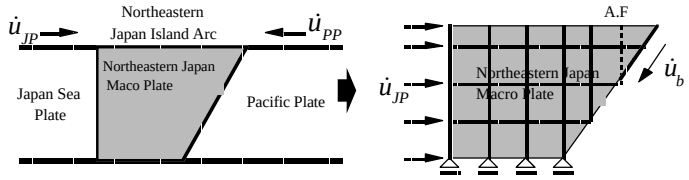

Figure 7: Schematics of the FEM model

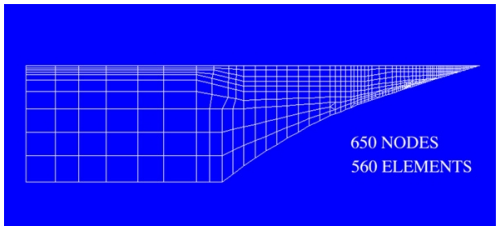

Figure 8: Mesh of the FEM model

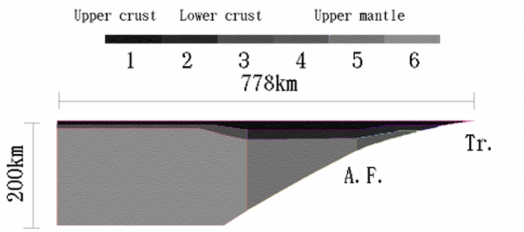

Material ID	Young's Modulus (N/m^2)	Poisson ratio	Coefficient of viscosity(N*s/m^2)
1	8.08E+10	0.226	Elastic
2	1.07E+11	0.258	1.0E+17
3	1.21E+11	0.258	1.0E+17
4	1.83E+11	0.245	1.0E+19
5	1.50E+11	0.273	1.0E+20
6	1.77E+11	0.273	1.0E+21

Figure 9: Material proprieties of the FEM model (the numbers under the colour bar correspond the material ID number in the table on the right side.)

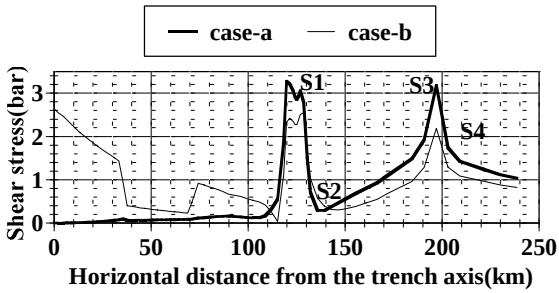

Figure 10: Accumulated shear stress calculated from the FEM model.

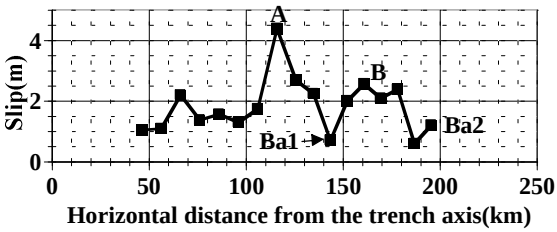

Figure 11: Slip obtained from the waveform inversion (Nakayama and Takeo(1997)). Labels A and B indicate the asperities shown in Figure 6. Labels Ba1 and Ba2 indicate the barriers.

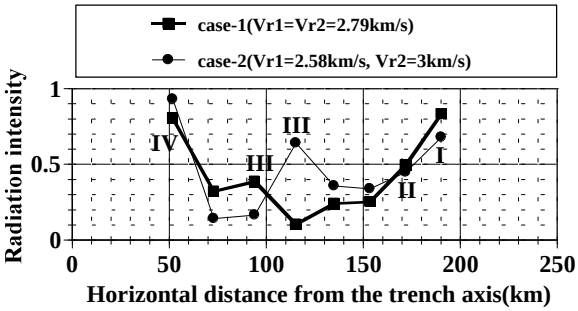

Figure 12: Acceleration radiation intensities obtained by the envelope inversion. Labels I, II, III, and IV are identical to those in Figure 4.

material properties and the size of the model are shown in Figure 9.

RESULTS

We calculated the shear stress field accumulated in the interval between the 1968 Tokachi-Oki earthquake and the 1994 Sanriku-Haruka-Oki earthquake. The numerical result is shown in Figure 10. This figure shows the maximum shear stress on the boundary of the Pacific Plate. The horizontal axis of the figure represents a horizontal distance from the Japan Trench axis. The direction of the distance is $N90^{\circ}W$. This direction is almost the same as that of the rupture propagation of the Sanriku-Haruka-Oki earthquake. The distribution patterns of the shear stress on the trenchward side bordered by the distance of about 120km depend strongly on the magnitude of C_f. Because of this result, we examine on the shear stresses only at the landward side of the border. For comparison, the maximum values of slip and acceleration radiation intensity among the subfaults in the same latitude are plotted in Figure 11 and 12 respectively. The horizontal axes of those figures are the same as Figure 9. The locations of the asperities A and B are also plotted in Figure 11.

The accumulated stress becomes lowest at a distance S2 (denoted in Figure 10) of about 135km from the trench and decreases rapidly with increasing distance in the extent beyond at a distance S3(denoted in the same figure) of 195km. The result suggests that the areas near to S2 and beyond S3 play a rule of a barrier. On the other hand, the accumulated stress becomes highest at a distance S1 (denoted in the same figure) of about 125km and increases with increasing distance in the extent from S2 to S3. The result suggests that the areas near to S1 and between S2 and S3 play a rule of an asperity. The suggestions of the results coincide with the results of the slip distributions shown in Figure 11 and 4: S2 coincides with the barrier Ba1 where the slip is lowest, the extent S4 beyond S3 coincides with the barrier Ba2 which lies beyond the western edge of the fault plane and stop the rupture, and the asperities A and B coincide with S1 and the extent from S2 and S3. The coincidence can be explained by the inference of Nakayama and Takeo (1997). From the their result that the asperity B overlaps with or is adjacent to the large slipped areas of the 1968 Tokachi-Oki earthquake, they inferred that the asperity B was a characteristic asperity.

The increase in accumulated stress in the area of asperity B (between S2 an S3) indicates that the rupture velocity increases as the rupture front approaches the western edge of the fault plane. This means that the rupture velocity at I (denoted in Figure 12) is higher than that at II (denoted in the same figure). Assuming that the rapid change in rupture velocity causes the high-frequency wave radiation at I and II, the intensity of high-frequency wave radiation is larger at I than at II. The assumption explains the fact that the acceleration radiation intensity is stronger at I than at II (see Figure 12). It is indicated that the spatial variation in accumulated stress in the asperity affects the intensity of the high-frequency wave radiation.

CONCLUSIONS

We examined the high-frequency wave radiation process of the 1994 Sanriku-Haruka-Oki earthquake and the accumulated tectonic stress on the source region with the envelope inversion method and the finite element model. The following results were obtained:

1) The large high-frequency waves were radiated at the edges of the fault plane and at the near edges of the large slipped area. This result suggests that stopping of rupture causes the high-frequency wave radiation.

2) The distribution pattern of accumulated stress on the western part of the fault plane is similar to that of slip. One of the possible explanations of the result is that the asperities on the western fault plane are characteristic asperities. This result suggests that the distribution pattern of asperity can be expected from the accumulated stress in the case of characteristic asperity. The distribution of accumulated stress was compared with that of high-frequency radiation intensity. It is indicated that the spatial variation in accumulated stress in the asperity affects the intensity of the high-frequency wave radiation.

The distribution of barriers and asperities controls the propagation and stopping of rupture. It is concluded that the prediction of the distribution in a source region is one of the important factors for the improvement of the prediction method of strong ground motion.

ACKNOWLEDGMENT

We acknowledge Wataru Nakayama and Minoru Takeo for providing us with the moment-rate data of the 1994 Sanriku-Haruka-Oki earthquake obtained from their inversion.

REFERENCES

Kakehi, Y. and K. Irikura (1996a), "Estimation of high frequency wave radiation area on the fault plane by the envelope inversion of acceleration seismograms", *Geohys. J. Int*., 125, pp892-900.

Kakehi, Y., K. Irikura, and M. Hoshiba (1996b). Estimation of high frequency wave radaiton area on the fault plane of the 1995 Hyogo-ken Nanbu earthquake by the envelope inversion of accleration seismograms", *J. Phys. Earth*, 44, pp505-517

Kakehi, T. and K. Irikura (1997), "High-frequency radation process during earthquake faulting - envelop inversion of accleration seismograms from the 1993 Hokkaido-Nansei-Oki, Japan, earthquake", *Bull. Seism. Soc. Am.*, 87, 904-917

Kato, K. and Takemura. M. (1996), "Rupture propagation of the 1994 Sanriku-Haruka-Oki earthquake deduced from the strong motion", *Zisin*, 49, pp75-83 (in Japanese)

Nakayama, W. and M.Takeo (1997), "Slip History of the 1994 Sanriku-Haruka-Oki, Japan, Earthquake Deduced from strong-motion Data", *Bull. Seism. Soc. Am*., 87, pp918-931

Sato, H., T. Nakahara, T. Nishimura, and M. Ohtake (1997), " Estimation of High-frequency Energy Radiation from an Earthquake Fault on the Basis of an envelope inversion method", *Proc. of the 2nd Symposium on Mitigation of Urban Disasters by Near-field Earthquake*, pp67-70 (in Japanese)

Sato. K. (1987), "Stress and displacement fields in the northeastern Japan Island Arc as evaluated with three-dimensional finite element method and their tectonic interpretations", *Doctor Thesis, Tohoku university*.